HHS Public Access

Author manuscript

Microcirculation. Author manuscript; available in PMC 2016 November 01.

Published in final edited form as:

Microcirculation. 2015 November ; 22(8): 724–736. doi:10.1111/micc.12247.

Right ventricular angiogenesis is an early adaptive response to chronic hypoxia-induced pulmonary hypertension

Todd M. Kolb, **Jacelyn Peabody**, **Philip Baddoura**, **Jon Fallica**, **Jason R. Mock**, **Benjamin D. Singer**, **Franco R. D'Alessio**, **Mahendra Damarla**, **Rachel L. Damico**, and **Paul M. Hassoun**

Division of Pulmonary and Critical Care Medicine, Department of Medicine, Johns Hopkins University, Baltimore, Maryland

Abstract

Objective—Myocardial angiogenesis is presumed to play a role in right ventricular (RV) adaptation to pulmonary hypertension (PH), though definitive evidence and functional correlations are lacking. We aimed to use definitive methods to correlate RV angiogenesis, hypertrophy, and function in a murine PH model.

Methods—Mice were exposed to chronic hypoxia for 21 days to induce PH (CH-PH) and RV remodeling. We used unbiased stereology and flow cytometry to quantify angiogenesis and myocyte hypertrophy, and pressure-volume loops to measure RV function.

Results—Within 7 days, RV-specific increases in total capillary length (10576±2574 cm vs. 6822±1379 cm; $P = 0.02$), surface area (10±3.3 cm^2 vs. 4.9±1.5 cm^2; $P = 0.01$), and volume (0.0013±0.0005 cm^3 vs. 0.0006±0.0001 cm^3; $P = 0.02$) were observed, and RV endothelial cell proliferation increased nearly 10-fold. Continued exposure led to progressive RV hypertrophy without additional angiogenesis. RV function was preserved, but activation of hypoxia-dependent gene expression was observed in both ventricles after 21 days.

Conclusions—Early RV remodeling in CH-PH is associated with RV angiogenesis and preserved RV function. Continued CH-PH is associated with RV hypertrophy but not angiogenesis, leading to biventricular activation of hypoxia-dependent gene expression.

Keywords

Pulmonary hypertension; stereology; angiogenesis; animal models

Introduction

Pulmonary hypertension (PH) is a serious complication of chronic cardiac and pulmonary disease. In some cases, subsequent right ventricular (RV) pressure overload can lead to RV failure and premature death. Indeed, RV dysfunction is a principal determinant of functional capacity and prognosis in PH, regardless of etiology [8, 16, 30]. The chronicity of PH allows

Corresponding Author: Todd M. Kolb, Division of Pulmonary and Critical Care Medicine, Johns Hopkins University School of Medicine, 1830 E. Monument Street, 5th Floor, Baltimore, MD 21205, toddkolb@jhmi.edu.

time for adaptive RV remodeling, characterized primarily by concentric hypertrophy with preserved RV function [22].

Current understanding of the mechanisms regulating adaptive RV remodeling in PH is incomplete. Hypertrophy of individual cardiac myocytes (CM), accompanied by obligate reorganization of the extracellular matrix is well accepted [3, 15]. In addition, RV-specific changes in myocyte gene expression (reversion to a "fetal gene program") [31] and transition to "glycolytic" metabolism (increased reliance on glucose as a substrate, increased glycolysis, reduced glucose oxidation) have been described [1]. As the metabolic demands of the anabolic myocardium increase, commensurate increases in myocardial perfusion are necessary. Angiogenesis has been convincingly demonstrated in animal models of left ventricular (LV) hypertrophy [27], however, the role of angiogenesis in RV adaptive remodeling is less clear.

Animal models of chronic hypoxia-induced PH (CH-PH) cause adaptive RV remodeling, with changes in RV capillary density (capillaries/mm^2) reported in some studies [13] but not others [21, 29]. Importantly, the methods used to quantify angiogenesis have intrinsic limitations that have led to variable interpretation. Relative growth of cardiac myocytes has been inconsistently considered in these assessments, and non-random sampling methods promote unintentional bias due to the complexity of the three-dimensional microvascular architecture. In PH models associated with RV failure (e.g., monocrotaline, MCT; VEGF receptor antagonist SU5416 combined with CH; Su/CH), reduced capillary density in the failing RV myocardium has been described [4, 21], suggesting an important association between the RV microcirculation and ventricular function. However, similar methodological issues exist in these studies, and the relationship between microvascular supply and RV contractility has not been explicitly explored.

In the present study, we tested the hypothesis that coordinate RV angiogenesis and myocyte hypertrophy occur during adaptive RV remodeling in a murine model of CH-PH, leading to preserved RV function. We combined unbiased stereological morphometric analyses and flow cytometry to measure angiogenesis in an effort to address some of the technical limitations of previous studies.

Method

Murine model of chronic-hypoxic pulmonary hypertension

Adult male C57 BL/6 mice (Jackson Laboratories; Bar Harbor, ME), aged 8–10 weeks, were exposed to normobaric hypoxia (10% O_2, balance nitrogen) for up to three weeks. Mice were housed in a ventilated plexiglass chamber, and nitrogen was added through a regulator (Pro-Ox 110; Biospherix; Lacona, NY) to maintain the O_2 concentration of ambient air in the chamber at 10%. Excess CO_2 was removed with soda lime. The chamber was opened twice weekly for cage changes. Food and water were available *ad libitum*. RV remodeling (hypertrophy) was quantified by measuring the mass ratio of the RV free wall to the LV and septum (Fulton Index). Pulmonary vascular remodeling was assessed semi-quantitatively in formalin-fixed, paraffin-embedded lung sections. Sections were stained with a monoclonal anti-human smooth muscle actin antibody (DAKO; Carpinteria, CA). The percentage of

visible vessels < 100 μm in diameter with full (continuous ring of SM-actin staining), partial (incomplete ring of SM-actin staining), and no (no SM-Actin staining) muscularization was determined in a blinded fashion from 6 randomly selected 10X fields per animal (5 animals/group). In total, greater than 300 vessels were counted per treatment condition. Venous blood hematocrit was measured following centrifugation in microcapillary tubes to assess hypoxia-induced polycythemia. For some experiments, mice were injected intraperitoneally with 60 mg/kg pimonidazole-HCl (Hypoxyprobe-1; Hypoxyprobe Inc.; Burlington, MA) one hour prior to harvesting tissue for assessment of tissue hypoxia. Pimonidazole-adducts were semi-quantitatively assessed by western blot given the higher sensitivity of this detection method (compared with immunohistochemistry), as previously reported [24].

Quantification of right ventricular angiogenesis

RV angiogenesis was quantified using stereological methods to estimate total RV capillary length, surface area, and volume. Mice were anesthetized with intraperitoneal pentobarbital (60 mg/kg). Heparin (0.1 mL of 0.05 U/μL) was injected into the vena cava and allowed to circulate for 2–3 minutes. The heart was arrested in diastole by injection of saturated potassium chloride into the vena cava, and mice were exsanguinated. Hearts were removed and preserved by immersion fixation in 10% formalin. Following removal of the atria and great vessels, the RV free wall was dissected from the septum and LV, and both ventricles were weighed. RV mass was converted to a reference volume by dividing by the density of muscle tissue (1.06 g/cm^3), as previously reported [5, 6, 32]. The RV was cut into 8–10 blocks of approximately 2 mm x 2 mm. Four blocks were chosen by systematic uniform random sampling; these were pre-embedded in spherical agarose molds to generate isotropic uniform random (IUR) sections in paraffin according to the isector method [19]. IUR sections on glass slides were de-paraffinized using xylene and a graded ethanol series, and stained with fluorophore-conjugated probes specific for endothelial cell glycoproteins (isolectin IB_4; Molecular Probes) and myocyte plasma membrane glycoproteins (wheat germ agglutinin; Molecular Probes), as previously described [14]. Digital images were obtained from ten 60-X fields per section, and stereological endpoints reflecting capillary length (profiles), surface (intersections), and volume (points) were quantified in a blinded manner using freely available software [28]. Counts were converted to tissue densities using the following equations:

1. length density = $2*Q/A_P * P_{RV}$
2. surface density = $2*I/L_P * P_{RV}$
3. volume density = $\Sigma P_{cap}/\Sigma P_{RV}$

Where Q = the number of capillary profiles counted, A_P = area represented by a probe point, P_{RV} = the number of points hitting the RV, I = the number of capillary intersections with line probes, L_P = the length of a line probe, and P_{cap} = the number of points hitting capillaries. Individual densities were then converted to total capillary length, surface, and volume by multiplying by the reference volume for each animal.

The number of animals, IUR sections, and images quantified for each experiment was determined by estimating the contribution of methodological error (versus true biological

variability) to the observed coefficient of variability for pilot experiments including 5 animals, 4 tissue blocks/animal, and 10 fields/ block. In this assessment, the contribution of methodological variability was <50% of the observed coefficient of variability for all measures, indicating that this approach was methodologically adequate [18].

Flow Cytometry

Mice exposed to normoxia or CH for 1 or 3-weeks were anesthetized with pentobarbital, exsanguinated, and hearts were removed for preparation of single cell suspensions. The RV free wall was dissected from the LV and septum. Both fractions were minced and incubated in RPMI media containing 0.25% collagenase I (Worthington Biochemical Corporation; Lakewood, NJ) and 0.05% DNase I (Sigma-Aldrich; Saint Louis, MO) for 45 minutes at 37 degrees. Suspensions were triturated through an 18-g needle and filtered through a 70 μm mesh prior to staining. Single cell suspensions were stained with the LIVE/DEAD Fixable Blue Cell Dead Stain Kit (Life Technologies; Grand Island, NY) and a Pacific Blue conjugated anti-mouse CD31 monoclonal antibody (Biolegend, Inc.; San Diego, CA) prior to fixation and permeabilization with the Foxp3/Transcription Factor Staining Buffer Set (eBiosicence, Inc.; San Diego, CA). Fixed and permeabilized single cell suspensions were subsequently stained with a PE-conjugated anti-human Ki-67 antibody (recognizes mouse Ki-67; BD Pharmingen; San Jose, CA). Matching isotype control antibodies were included for each stain. Right and left ventricular cell suspension were then subjected to flow cytometry using a FACSAria cell sorter and analyzer (BD Biosciences), and data were analyzed using FlowJo software (v. 7.6.5; Ashland, OR). The percentage of live, $CD31^+$ cells staining positively for Ki-67 was used as a measure of endothelial cell proliferation.

Measurement of RV hemodynamics

Mice were anesthetized with intraperitoneal pentobarbital (60 mg/kg) and mechanically ventilated with the following parameters: tidal volume = 10 ml/kg; rate = 160 breaths*min^{-1}). Temperature was maintained at 37° C (±0.4°) using a heating pad controlled by a proportional-integral-derivative temperature control unit (Doccol; Sharon, MA). The apex of the heart was exposed by diaphragmotomy, and a 1.2F P-V catheter (Transonic Systems, Inc.; Ithaca, NY) was inserted into the RV. Instantaneous pressure and electrical conductance signals were obtained and recorded on a PowerLab data acquisition system (ADInstruments, Inc.; Colorado Springs, CO), and the conductance signal was converted to a volume estimate using a proprietary algorithm through the ADVantage pressure-volume control unit (Transonic). The stroke volume estimate (25 μL) used in this algorithm was consistent with previous reports in the literature [20], and was confirmed via direct measurement of cardiac output at the ascending aorta using a 1.5 mm perivascular flow probe (Transonic, Inc.). After loops were generated from anesthetized animals in the steady state, we measured pressure-volume loops during inferior vena cava occlusion through manual compression. Data were recorded and analyzed using LabChart 7 software (ADInstruments, Inc.).

Measurement of RV protein and RNA expression

RV free wall and LV/septal specimens were flash-frozen immediately after euthanasia for measurement of protein and RNA expression. Tissue homogenates were prepared in RIPA

Lysis and Extraction Buffer (protein; Thermo Fisher Scientific, Inc.; Rockford, IL) or Trizol Reagent (RNA; Thermo Fisher Scientific, Inc.) using the Bullet Blender Homogenizer cell disrupter (Next Advance, Inc.; Averill Park, NY). Protein lysates were used for ELISA (mouse VEGF Quantikine ELISA, R&D Systems; Minneapolis, MN) or western blotting using commercially available antibodies directed against pimonidazole adducts (PAb2627 ;Hypoxyprobe, Inc.; Burlington, MA) or hsp90 (Cell Signaling Technologies; Beverly, MA). Image J software (NIH) was used to quantify band density. Total RNA was further extracted with chloroform, precipitated with isopropanol, and washed with ethanol prior to purification with the RNeasy kit (QIAgen; Germantown, MD). Purified RNA was used to generate cDNA using the RT2 First Strand system (QIAgen). Quantitative PCR was performed using primers specific for mouse VEGFa (forward = TGTGCGCAGACAGTGCTCCA; reverse = AGCCTGGGACCACTTGGCAT), VEGFb (forward = AAAGGAGAGTGCTGTGAAGCCAGA; reverse = TGGAAAGCAGCTTGTCACTTTCGC), and hsp90 (forward = TCGGCTTTCCCGTCAAGATGCC; reverse = AGAAGGGTCCGTCAGGCTCTCA), generated using the Primer-BLAST program freely available through the National Center for Biotechnology Information website (www.ncbi.nlm.nih.gov). Relative changes in gene expression were quantified using REST 2009 (QIAgen), with significant changes quantified using a pairwise reallocation randomization test. Global expression profiles of hypoxia-dependent gene expression were measured by quantitative PCR using the Mouse Hypoxia Signaling Pathway PCR array (QIAgen), and relative changes in gene expression were quantified using the $\Delta\Delta C_t$ method via RT2 Profiler PCR Array Data Analysis software (version 3.5; QIAgen).

Statistical Analysis

Comparison of means between two groups was made using an unpaired t-test, with Welch's correction in the setting of unequal variances, as appropriate. Comparison of means between control groups and CH-exposed groups at multiple time points was made using one-way ANOVA, with *post-hoc* testing corrected for multiple comparisons using Dunnett's test. In experiments where time represented a second variable, two-way ANOVA was used to compare differences between group means. Comparison of proportions of muscularized and non-muscularized pulmonary vessels was made via Pearson's chi-square test. A two-tailed P value < 0.05 was considered statistically significant in all experiments. Statistical analyses were performed using GraphPad Prism software (v 6.04; GraphPad Software, Inc.; La Jolla, CA).

Results

Chronic hypoxia induces progressive RV hypertrophy

RV-specific hypertrophy (RVH) is a well-described response to chronic hypoxia in mice, and is routinely quantified as the ratio of RV mass to LV/septal mass (Fulton index) or as the ratio of RV mass to body mass. As shown in Figure 1A, Fulton index is significantly increased after 7 days of exposure to CH, with further increases in RVH noted after 21 days of CH. RVH measured by RV mass/body mass ratio was similarly increased after 1 and 3

weeks of CH, though CH significantly reduced time-dependent body weight gain (Table 1). CH exposure did not increase LV/septal mass at any time point (Table 1).

CH-induced RVH has classically been associated with muscular remodeling of small (< 100 μm) pulmonary arteries. In our studies, significantly increased proportions of partially- and fully-muscularized small pulmonary vessels were observed after 1 week of CH, as anticipated ($P < 0.0001$; Fig. 1B).

Effects of CH-PH on myocardial angiogenesis

We used unbiased stereological methods to estimate the total capillary length, surface area, volume, and CM volume in mouse RV and LV/S under normoxic and CH conditions. Figure 2A shows representative images of IUR sections, stained for endothelial cells (IB_4) and CM membranes (WGA). As shown in Figure 2B, 7 days of CH was associated with a 25% increase in RV CM volume. The increase in RV CM volume was proportional to the observed 29 % increase in RV volume ($V_{RV,}$ Table 2). Significant increases in estimated RV capillary length (55%), surface area (110%), and volume (117%) were observed after 7 days of CH (Figure 2C and Table 2). There was no increase in measured LV/S volume or estimated LV CM volume, capillary length, capillary surface area, or capillary volume after 1 week of CH (Figure 3).

After 21 days of CH-PH, we also observed significant increases in estimated RV CM volume, capillary length, capillary surface area, and capillary volume (Table 2). When compared to estimates obtained after 7 days of CH (by 2-way ANOVA), the effects of CH on microcirculatory or myocyte parameters were not further altered by 21 days of CH (Table 2). Similarly, changes in stereological parameters were not observed in mouse LV/S after 21 days of CH (Table S1).

Relative growth of RV CM and capillaries in CH-PH

The relationship between CM growth (hypertrophy) and myocardial perfusion is complex. CH-PH has the potential to regulate CM hypertrophy, myocardial angiogenesis, and myocardial blood flow independently. We compared relative changes in capillary stereological parameters induced by CH-PH to changes in CM volume. In the RV, total capillary length, surface, and volume each demonstrated robust, positive correlations with CM volume (Table 3). In the LV, there was no correlation between CM volume and any microcirculatory parameter measured. We subsequently used linear regression of logarithmically transformed data to calculate an index of relative growth (allometry coefficient, **a**) between each capillary parameter and CM volume.

Proportionate growth (isometry) would theoretically be reflected by an allometry coefficient $a=1$, with values of $a > 1$ reflecting proportionately higher growth rates in capillary parameters. As shown in Figure 4, capillary length, surface, and volume each demonstrated allometry coefficients significantly greater than 1, suggesting that CH-PH induced increases in each capillary parameter exceeds CH-PH induced increases in CM volume. When compared against one another, the allometry coefficients were not significantly different ($P = 0.34$), suggesting statistically similar rates of relative growth among all microcirculatory

parameters (when compared with CM volume). Similar analyses were not performed in the LV, given any lack of association between CM volume and capillary indices (Table 3).

CH-PH induced increases in RV capillary length are associated with RV endothelial cell proliferation

To confirm that observed increases in RV capillary length were the result of sprouting angiogenesis (as opposed to recruitment of non-distended capillaries), we measured myocardial endothelial cell (EC) proliferation in RV and LV/S single cell suspensions. EC proliferation is required for sprouting angiogenesis, and we hypothesized that increased capillary length would be associated with EC proliferation in this model. We used flow cytometry to identify viable $CD31^+$ cells, and quantified the percentage of these cells staining positively for the proliferation marker Ki-67. Consistent with our stereological analyses, we observed a robust (~10 fold) increase in RV $CD31^+$ cell proliferation after 7 days of CH, but not after 21 days of CH (Figure 5). No significant change in LV/S $CD31^+$ cell proliferation was noted at either time point. These findings confirm an RV-specific increase in EC proliferation in response to CH-PH, and are temporally consistent with observed changes in RV capillary length (increased by 7 days, plateaued at 21 days) noted above (Table 2).

CH-PH associated hemodynamic changes

Simultaneous measures of RV pressure and volume throughout the cardiac cycle, made at rest and during inferior vena cava (IVC) occlusion, were used to assess RV hemodynamics (Table 4) during CH-PH induced RV remodeling to assess the relationship between RV angiogenesis and RV function. Measurements were obtained under similar levels of sedation, and temperature was strictly controlled in each group, as reflected by the consistent heart rates. CH-PH caused significant increases in RV end-systolic pressure (ESP) after 7 days, with no further increases after 21 days. Increased RV pressure was associated with a modest increase in effective arterial elastance (E_a; reflecting total RV afterload) after 7 days of CH-PH, though this increase did not quite meet statistical significance. Stroke volume and cardiac output were preserved after 7 and 21 days of CH-PH. RV end-diastolic pressure (EDP) was increased after 21 days of CH-PH, though end-diastolic volume (EDV) did not change significantly.

Systolic function did not change dramatically with CH-PH. While there were significant increases in dP/dt_{max} and stroke work, load-independent measures of RV contractility (end-systolic elastance, preload recruitable stroke work, dP/dt_{max}-EDV relationship) did not change with CH-PH. These findings suggest that RV contractility was preserved, but did not increase during RV remodeling in this model. Importantly, RV-PA coupling (as reflected by the ratio of end-systolic elastance to effective arterial elastance; E_{es}/E_a) was preserved. Effects on lusitropy were conflicting, with CH-PH induced increases in dP/dt_{min} (load-dependent measure of isovolumic relaxation), but no change in Tau (preload-independent measure of isovolumic relaxation).

CH-PH associated RV remodeling is associated with late ventricular tissue hypoxia

Mice exposed to CH developed tissue-specific hypoxic adaptations within 1 week, as evidenced by significant increases in hematocrit (Figure 6C). RV tissue hypoxia could similarly provide a stimulus for myocardial angiogenesis in the CH-PH model. We measured RV tissue hypoxia and VEGF expression to determine whether these factors were associated with, and potentially regulators of, RV angiogenesis in the CH-PH model.

Tissue hypoxia was assessed by pimonidazole staining and measurement of hypoxia-inducible gene expression. Pimonidazole forms adducts with proteins and amino acids when tissue partial pressure of O_2 falls below 10 mm Hg; these adducts are detectable via Western blot. As shown in Figure 6, RV pimonidazole adduct (PAb2627) staining did not increase significantly during the first week of CH-PH. Instead, RV pimonidazole adduct formation was significantly reduced after 7 days of CH-PH when compared to normoxic mice. LV pimonidazole staining did not change during the first week of CH-PH. Pimonidazole adduct formation was increased in both ventricles after 21 days of CH-PH (not shown).

We subsequently used microarray-based quantitative PCR to measure changes in hypoxia-regulated gene expression in RV and LV homogenates from mice exposed CH-PH for 7 or 21 days. In the RV (Table 5), only one (*Ier3*; immediate early response-3) of 85 possible genes was up-regulated in mice exposed to CH-PH for 1 week. However, robust increases in hypoxic gene expression were noted in RV samples after 3 weeks of CH-PH. In total, expression of 34 of 85 possible genes was significantly altered when compared to normoxic RV. Of these, 17 (Table 5) were up-regulated > 1.5 fold. Three of these genes were uniquely up-regulated by CH in the RV: cyclin G2 (*Ccng2*), lactate dehydrogenase A (*Ldha*), and mitogen-activated protein kinase kinase kinase 1 (*Map3k1*). In the LV, hypoxia-dependent gene expression was not significantly altered after 7 days of CH-PH (Table S2). The eukaryotic translation initiation factor 4E binding protein 1 (*Eif4ebp1*) and plasminogen activator, urokinase (*Plau*) were significantly down-regulated in LV homogenates after 7 days of CH. After 21 days of CH, however, LV expression of 25 of 85 possible genes was significantly altered when compared to normoxic LV, and 16 of these were up-regulated > 1.5-fold (Table S2). Four of these, Ankyrin repeat domain 37 (*Ankrd37*), coagulation factor III (*F3*), heme oxygenase 1 (*Hmox1*), and solute carrier family 16, member 3 (*Slc16a3*), were uniquely up-regulated in CH LV.

We subsequently measured RV and serum VEGF expression to determine whether this classical pro-angiogenic growth factor was upregulated during CH-PH induced RV angiogenesis. Quantitative PCR demonstrated no significant change in VEGF-α or VEGF-β RNA during the first 21 days of RV remodeling (Figure 7A). Similarly, ELISA demonstrated no increase in RV VEGF protein expression after 7 days of CH-PH; however, RV VEGF was significantly increased at the 21 day time point (Figure 7B), temporally consistent with microarray data demonstrating hypoxic gene activation at this time point. There were trends towards increased serum levels of VEGF after 7 and 21 days of CH-PH, though these differences did not reach statistical significance (Figure 7C).

Discussion

Using a murine model of chronic hypoxic pulmonary hypertension, we have demonstrated that myocardial angiogenesis is an early, RV-specific process in adaptive remodeling. In this study, RV angiogenesis was defined by increases in total capillary length and concomitant RV endothelial cell proliferation. These adaptations were accompanied by increased RV capillary surface area and volume, suggesting increased area for tissue diffusion and increased RV blood volume, respectively. RV microvascular adaptations and RV myocyte hypertrophy were tightly associated, while there was no association between capillary parameters and myocyte volume in the LV. Interestingly, continued exposure to CH led to progressive RVH without continued RV angiogenesis, ultimately resulting in activation of hypoxia-dependent gene expression in both ventricles. Importantly, RV function (including RV-PA coupling) was preserved throughout.

By combining unbiased stereology and evidence of concomitant RV EC proliferation, we believe this study provides the strongest evidence to date of RV angiogenesis in an animal model of PH. Previous studies have relied primarily on simple counting of capillary profiles in 2-D tissue sections [4, 13, 21, 29], which may lead to underestimation of effective capillary length and surface area [11] (due to the complex three-dimensional structure of the reticular capillary network) and unintentional sampling bias (due to intrinsic variability in capillary density within the myocardium [11, 12]). Previous reports have also been difficult to interpret and inconsistent, with variable reports of unchanged [21, 29] or increased [13] capillary density in the same model (CH-PH). Furthermore, the endpoints obtained using stereological methods are more intuitive, and provide significantly more information for structure-function relationships, with many well-validated endpoints described for cardiac physiology (as recently reviewed [18]). Despite these benefits, stereological methods are slowly being incorporated into studies focused on the myocardial vascular supply, and most of the available information is limited to the LV (reviewed in [17]). Importantly, our estimates of LV CM volume, LV capillary length, and LV capillary surface area are consistent with those recently reported for C57 BL/6 mice [9, 10], extending this burgeoning literature.

More recently, advanced methods (including three-dimensional reconstruction of confocal images after fluorescent lectin perfusion) were used to demonstrate a potential early increase in RV microvasculature (as quantified by increased fluorescence), followed by late normalization as failure ensued in the MCT model [26]. Similar methods were used to demonstrate a late decline in RV microvascular “volume” and capillary density in the Su/CH model of pulmonary hypertension [4]. While these approaches addressed some of the considerations regarding anisotropy and complexity of the RV microvasculature, they remain subject to unintentional bias due to non-random sampling methods. However, these studies, combined with our current observations, strongly suggest that myocardial angiogenesis is an important early component of RV adaptation to PH.

Endothelial cell activation and proliferation are necessary for sprouting angiogenesis. Therefore demonstration of active RV endothelial cell proliferation in this model, temporally consistent with increases in RV capillary length, is highly consistent with

sprouting angiogenesis as the mechanism for early microvascular growth. Importantly, the establishment of this cellular marker (EC proliferation) provides a temporal framework for future studies aimed at understanding the molecular regulators and physiological stimuli for RV angiogenesis during adaptive remodeling. In the CH-PH model, relevant pro-angiogenic mediators should be activated during the first week of exposure to CH-PH. As an example, we measured RV VEGF mRNA and protein expression during the first week of adaptive remodeling. Surprisingly, we observed no statistically significant increase in early RV VEGF mRNA or protein expression (though there was a modest, nearly significant increase in VEGFα mRNA at 1 day). Previous studies have demonstrated VEGF to be a potential regulator of myocardial angiogenesis in PH and other models of pressure-overload induced myocardial remodeling [4, 23, 25], and our data do not exclude VEGF as a regulator of early angiogenesis in CH-PH (as VEGF receptor levels/activation were not measured). Additional mechanistic studies, focused on VEGF receptor expression/phosphorylation and other pro-angiogenic growth factors (e.g., fibroblast growth factor, placenta growth factor) known to regulate VEGF-independent angiogenesis [7] are clearly warranted. We believe the present study provides the critical methodological and temporal framework to explore these important questions.

This study also reports allometry coefficients for the relationships between RV microvascular growth and RV CM volume. Although we would not argue that the reported coefficients represent absolute numerical relationships between microvascular growth and myocyte growth (due to small sample sizes), we hypothesize that this approach will allow quantification of relative RV angiogenesis between PH models or when regulators of angiogenesis or hypertrophy are experimentally manipulated in a PH model. Allometric coefficients mathematically describe the scaling relationships between biological traits or physiological processes, and have been used in previous studies of comparative tissue angiogenesis [33]. In our studies, all microcirculatory parameters increased at a rate exceeding CM growth, but did not differ significantly from each other. These results suggest that angiogenesis (increased capillary length) and increased blood flow (increased volume and surface area) are likely both important early RV circulatory adaptations to PH.

Functionally, early RV angiogenesis (1 week) was associated with preserved RV function and protection from tissue hypoxia in this model. Surprisingly, continued hypertrophy without concomitant angiogenesis was observed, and was associated with activation of hypoxic gene expression in both ventricles after 3 weeks of CH-PH. Many of the induced genes regulate glycolytic metabolism. The consequences of glycolytic metabolism in RV remodeling are unclear, with several lines of evidence suggesting that this seemingly adaptive change may in fact be detrimental (reviewed in [22]).The mechanisms leading to uncoupling of RV angiogenesis and myocyte hypertrophy in this model warrant further investigation, and may include inhibition of pro-angiogenic signals and/or up-regulation of angiostatic mediators.

There are several limitations to our study. Primarily, these studies are descriptive, and do not define angiogenesis as necessary or sufficient for adaptive RV remodeling. However, we feel these findings provide essential information by establishing a model and methodological structure for future mechanistic studies. We have also used the CH-PH model, which has

been criticized as poorly representative of human PAH due to its mild phenotype with only modest pulmonary vascular remodeling and lack of progression to RV failure. However, we feel that preservation of RV function is a strength when testing hypotheses regarding basic mechanisms of early, adaptive remodeling. Candidate regulatory proteins can subsequently be assessed in more robust models of PH associated with RV failure to clarify their roles in maintenance of myocardial compensation. As an example, quantification of early angiogenesis in the MCT or Su/CH model will allow clarification of whether or not previously described "capillary rarefaction" is indeed an intrinsic EC loss or a failure of early angiogenesis. We also focused on two unique time points for the stereological and flow cytometry studies. However, these time points were sufficient to generate a temporal framework for RV angiogenesis in CH-PH, and exploration of additional time points would be too labor intensive to justify. We did not use CD45 staining to exclude $CD31^+/CD45^+$ leukocytes from our analysis of EC proliferation in these experiments. However, we have included CD45 staining in similar experiments and found that a $CD31^+/CD45^+$ population is consistently undetectable in the RV after one or three weeks of CH-PH (not shown). Moreover, as observed increases in $CD31^+$ cell proliferation were temporally and regionally consistent with stereologically measured increases in capillary length, and as the observed percentage of $CD31^+$ cells in RV homogenates in these experiments was consistent with the previously reported percentage of endothelial cells in adult murine myocardium [2], we believe the use of CD31 staining is a reasonably specific marker for EC in this study. Finally, we did not measure additional markers of anaerobic metabolism/glycolysis in this study. These critical mechanistic correlates of the current observations are the subject of ongoing studies.

In summary, we have used a novel combination of unbiased stereological methods and flow cytometry to establish RV angiogenesis as an early event in a murine PH model of adaptive remodeling. We think these findings represent a critical first step in clarifying the physiologic and molecular events that coordinate the complex process of myocardial vascular remodeling during pulmonary hypertension.

Supplementary Material

Refer to Web version on PubMed Central for supplementary material.

Acknowledgements

Jason R. Mock is presently affiliated with the Division of Pulmonary Diseases and Critical Care Medicine, Department of Medicine, University of North Carolina, Chapel, Hill, NC. The authors would like to thank Drs. Wayne Mitzner (Johns Hopkins School of Public Health), Rubin Tuder (University of Colorado), and Abigail Lara (University of Colorado) for their helpful guidance regarding design based stereological methods, and Mr. Raffaello Cimbro (Johns Hopkins University) for his technical expertise in flow cytometry methods and analysis.

Perspectives: This study provides quantitative evidence of early RV angiogenesis in a PH model, and correlates changes in the RV microvasculature with measures of myocardial function and remodeling. The results show that angiogenesis is an early, adaptive, and RV-specific response to CH-PH. Importantly, the study establishes a model, methodological structure, and temporal framework for more detailed mechanistic studies that will provide insight into the stimuli and molecular regulators of RV angiogenesis during adaptive remodeling in PH. Ultimately, these findings may lead to the identification of novel biomarkers and/or therapeutic targets for RV remodeling in PH.

Supported by grants from the National Heart, Lung and Blood Institute (R01 HL114910, P.M.H., and F32 HL 110516, T.K.); American Heart Association (FTF17220008, T.K.) and Pulmonary Hypertension Association/ American Thoracic Society (Career Development Award 90052837, T.K.).

List of Abbreviations

ANOVA	analysis of variance
CH-PH	chronic hypoxic pulmonary hypertension
CM	cardiac myocyte
EC	endothelial cell
EDP	end-diastolic pressure
EDV	end-diastolic volume
ESP	end-systolic pressure
IB_4	isolectin B_4
IUR	isotropic uniform random
IVC	inferior vena cava
LV	left ventricle
MCT	monocrotaline
PH	pulmonary hypertension
RV	right ventricle
RVH	right ventricular hypertrophy
SM	smooth muscle
Su/CH	Sugen 5416 combined with chronic hypoxia
VEGF	vascular endothelial growth factor
WGA	wheat germ agglutinin

References

1. Abel ED, Doenst T. Mitochondrial adaptations to physiological vs. pathological cardiac hypertrophy. Cardiovasc Res. 2011; 90:234–242. [PubMed: 21257612]
2. Banerjee I, Fuseler JW, Price RL, Borg TK, Baudino TA. Determination of cell types and numbers during cardiac development in the neonatal and adult rat and mouse. Am J Physiol Heart Circ Physiol. 2007; 293:H1883–H1891. [PubMed: 17604329]
3. Bogaard HJ, Abe K, Vonk NA, Voelkel NF. The right ventricle under pressure: cellular and molecular mechanisms of right-heart failure in pulmonary hypertension. Chest. 2009; 135:794–804. [PubMed: 19265089]
4. Bogaard HJ, Natarajan R, Henderson SC, Long CS, Kraskauskas D, Smithson L, Ockaili R, McCord JM, Voelkel NF. Chronic pulmonary artery pressure elevation is insufficient to explain right heart failure. Circulation. 2009; 120:1951–1960. [PubMed: 19884466]
5. Bruel A, Oxlund H, Nyengaard JR. Growth hormone increases the total number of myocyte nuclei in the left ventricle of adult rats. Growth Horm IGF Res. 2002; 12:106–115. [PubMed: 12175648]

6. Eisele JC, Schaefer IM, Randel NJ, Post H, Liebetanz D, Bruel A, Muhlfeld C. Effect of voluntary exercise on number and volume of cardiomyocytes and their mitochondria in the mouse left ventricle. Basic Res Cardiol. 2008; 103:12–21. [PubMed: 18004633]
7. Ferrara N. Pathways mediating VEGF-independent tumor angiogenesis. Cytokine Growth Factor Rev. 2010; 21:21–26. [PubMed: 20005148]
8. Ghio S, Gavazzi A, Campana C, Inserra C, Klersy C, Sebastiani R, Arbustini E, Recusani F, Tavazzi L. Independent and additive prognostic value of right ventricular systolic function and pulmonary artery pressure in patients with chronic heart failure. J Am Coll Cardiol. 2001; 37:183–188. [PubMed: 11153735]
9. Gruber C, Kohlstedt K, Loot AE, Fleming I, Kummer W, Muhlfeld C. Stereological characterization of left ventricular cardiomyocytes, capillaries, and innervation in the nondiabetic, obese mouse. Cardiovasc Pathol. 2012; 21:346–354. [PubMed: 22197049]
10. Gruber C, Nink N, Nikam S, Magdowski G, Kripp G, Voswinckel R, Muhlfeld C. Myocardial remodelling in left ventricular atrophy induced by caloric restriction. J Anat. 2012; 220:179–185. [PubMed: 22077432]
11. Hudlicka O, Brown M, Egginton S. Angiogenesis in skeletal and cardiac muscle. Physiol Rev. 1992; 72:369–417. [PubMed: 1372998]
12. Kaneko N, Matsuda R, Toda M, Shimamoto K. Three-dimensional reconstruction of the human capillary network and the intramyocardial micronecrosis. Am J Physiol Heart Circ Physiol. 2011; 300:H754–H761. [PubMed: 21148764]
13. Kayar SR, Banchero N. Myocardial capillarity in acclimation to hypoxia. Pflugers Arch. 1985; 404:319–325. [PubMed: 4059024]
14. Koitabashi N, Danner T, Zaiman AL, Pinto YM, Rowell J, Mankowski J, Zhang D, Nakamura T, Takimoto E, Kass DA. Pivotal role of cardiomyocyte TGF-beta signaling in the murine pathological response to sustained pressure overload. J Clin Invest. 2011; 121:2301–2312. [PubMed: 21537080]
15. Kret M, Arora R. Pathophysiological basis of right ventricular remodeling. J Cardiovasc Pharmacol Ther. 2007; 12:5–14. [PubMed: 17495253]
16. Mohammed SF, Hussain I, Abou Ezzeddine OF, Takahama H, Kwon SH, Forfia P, Roger VL, Redfield MM. Right ventricular function in heart failure with preserved ejection fraction: a community-based study. Circulation. 2014; 130:2310–2320. [PubMed: 25391518]
17. Muhlfeld C. Quantitative morphology of the vascularisation of organs: A stereological approach illustrated using the cardiac circulation. Ann Anat. 2014; 196:12–19. [PubMed: 23290457]
18. Muhlfeld C, Nyengaard JR, Mayhew TM. A review of state-of-the-art stereology for better quantitative 3D morphology in cardiac research. Cardiovasc Pathol. 2010; 19:65–82. [PubMed: 19144544]
19. Nyengaard JR, Gundersen HJ. The isector: a simple and direct method for generating isotropic, uniform random sections from small specimens. J Microsc. 1992; 165:427–431.
20. Pacher P, Nagayama T, Mukhopadhyay P, Batkai S, Kass DA. Measurement of cardiac function using pressure-volume conductance catheter technique in mice and rats. Nat Protoc. 2008; 3:1422–1434. [PubMed: 18772869]
21. Partovian C, Adnot S, Eddahibi S, Teiger E, Levame M, Dreyfus P, Raffestin B, Frelin C. Heart and lung VEGF mRNA expression in rats with monocrotaline- or hypoxia-induced pulmonary hypertension. Am J Physiol. 1998; 275:H1948–H1956. [PubMed: 9843792]
22. Ryan JJ, Archer SL. The right ventricle in pulmonary arterial hypertension: disorders of metabolism, angiogenesis and adrenergic signaling in right ventricular failure. Circ Res. 2014; 115:176–188. [PubMed: 24951766]
23. Sano M, Minamino T, Toko H, Miyauchi H, Orimo M, Qin Y, Akazawa H, Tateno K, Kayama Y, Harada M, Shimizu I, Asahara T, Hamada H, Tomita S, Molkentin JD, Zou Y, Komuro I. p53-induced inhibition of Hif-1 causes cardiac dysfunction during pressure overload. Nature. 2007; 446:444–448. [PubMed: 17334357]
24. Sato Y, Endo H, Okuyama H, Takeda T, Iwahashi H, Imagawa A, Yamagata K, Shimomura I, Inoue M. Cellular hypoxia of pancreatic beta-cells due to high levels of oxygen consumption for insulin secretion in vitro. J Biol Chem. 2011; 286:12524–12532. [PubMed: 21296882]

25. Shiojima I, Sato K, Izumiya Y, Schiekofer S, Ito M, Liao R, Colucci WS, Walsh K. Disruption of coordinated cardiac hypertrophy and angiogenesis contributes to the transition to heart failure. J Clin Invest. 2005; 115:2108–2118. [PubMed: 16075055]

26. Sutendra G, Dromparis P, Paulin R, Zervopoulos S, Haromy A, Nagendran J, Michelakis ED. A metabolic remodeling in right ventricular hypertrophy is associated with decreased angiogenesis and a transition from a compensated to a decompensated state in pulmonary hypertension. J Mol Med (Berl). 2013; 91:1315–1327. [PubMed: 23846254]

27. Tomanek RJ. Response of the coronary vasculature to myocardial hypertrophy. J Am Coll Cardiol. 1990; 15:528–533. [PubMed: 1689327]

28. Tschanz SA, Burri PH, Weibel ER. A simple tool for stereological assessment of digital images: the STEPanizer. J Microsc. 2011; 243:47–59. [PubMed: 21375529]

29. Turek Z, Hoofd LJ, Ringnalda BE, Rakusan K. Myocardial capillarity of rats exposed to simulated high altitude. Adv Exp Med Biol. 1985; 191:249–255. [PubMed: 2938451]

30. van de Veerdonk MC, Kind T, Marcus JT, Mauritz GJ, Heymans MW, Bogaard HJ, Boonstra A, Marques KM, Westerhof N, Vonk-Noordegraaf A. Progressive right ventricular dysfunction in patients with pulmonary arterial hypertension responding to therapy. J Am Coll Cardiol. 2011; 58:2511–2519. [PubMed: 22133851]

31. Voelkel NF, Quaife RA, Leinwand LA, Barst RJ, McGoon MD, Meldrum DR, Dupuis J, Long CS, Rubin LJ, Smart FW, Suzuki YJ, Gladwin M, Denholm EM, Gail DB. Right ventricular function and failure: report of a National Heart, Lung, and Blood Institute working group on cellular and molecular mechanisms of right heart failure. Circulation. 2006; 114:1883–1891. [PubMed: 17060398]

32. Wulfsohn D, Nyengaard JR, Tang Y. Postnatal growth of cardiomyocytes in the left ventricle of the rat. Anat Rec A Discov Mol Cell Evol Biol. 2004; 277:236–247. [PubMed: 14983518]

33. Young S, Egginton S. Allometry of skeletal muscle fine structure allows maintenance of aerobic capacity during ontogenetic growth. J Exp Biol. 2009; 212:3564–3575. [PubMed: 19837898]

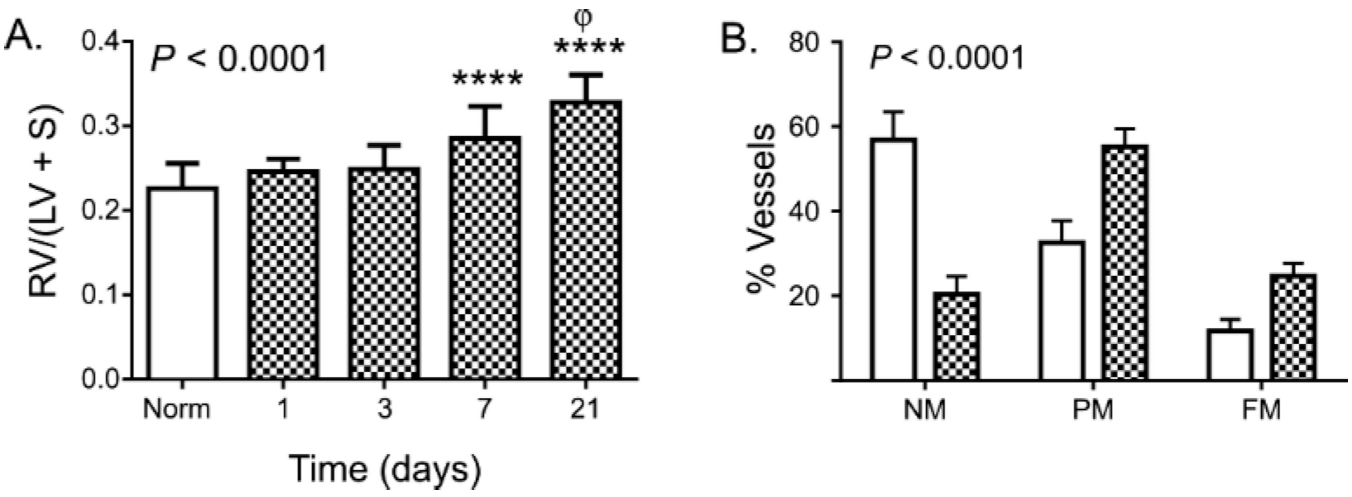

Figure 1. Chronic hypoxia induces progressive RVH

In (A), RVH is measured as the ratio of RV mass to LV + septum mass at each time point. Mean and standard deviation are shown at each time point, with normoxic data pooled from all experiments. Replicate numbers as outlined in Table 1. *P* value is for ANOVA; **** = $P < 0.0001$ between CH and control, $\Phi = P < 0.01$ between 21 days and 7 days (corrected for multiple comparisons). In (B), the proportion of small pulmonary vessels (< 100 μm) that are non- (NM), partially- (PM), or fully-muscularized (FM) are shown in mice exposed to normoxia or chronic hypoxia for 1 week. At least 340 vessels were counted per treatment condition. P value is for differences among groups via χ^2.

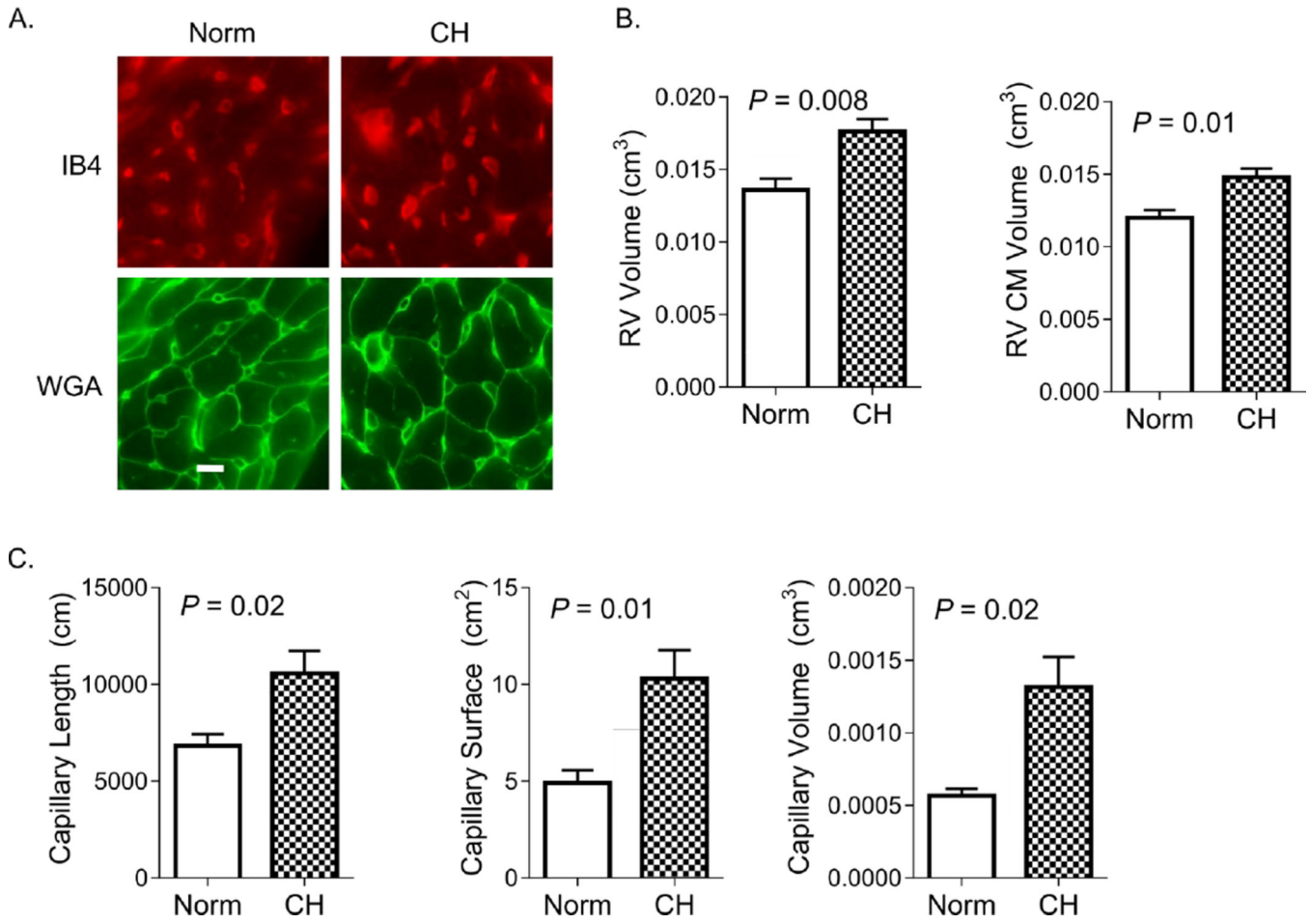

Figure 2. Chronic hypoxia induces early RV angiogenesis

In (A), representative images of RV isotropic uniform random (IUR) sections stained with markers specific for endothelial cell glycoproteins (isolectin IB_4) and myocyte plasma membrane glycoproteins (wheat germ agglutinin; WGA) are shown. IB4 stains endothelial cells of capillaries and larger resistance vessels, though only the former were quantified. Bar = 10 μm. Images were used for stereological assessment in animals exposed to normoxia (Norm) and chronic hypoxia (CH) for 7 days. In (B), RV volume and RV CM volume increase with CH. As shown in (C), RV capillary length, surface area, and luminal volume are significantly increased after 7 days of CH. *P*-values are for Student's t-test.

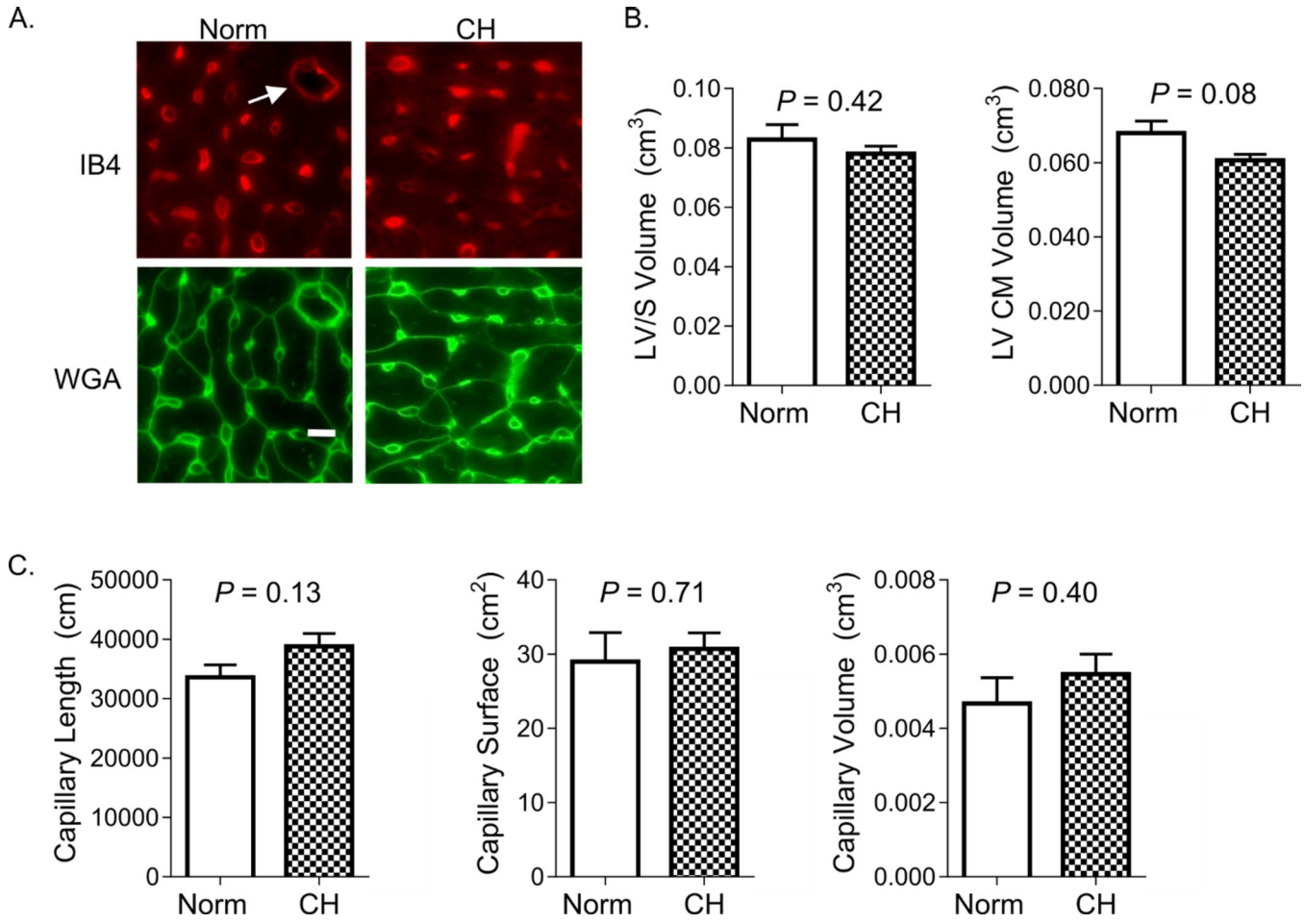

Figure 3. LV angiogenesis does not occur during CH-PH induced RV remodeling

In (A), representative images of LV/septum stained with markers specific for endothelial cell glycoproteins (isolectin IB_4) and myocyte plasma membrane glycoproteins (wheat germ agglutinin; WGA) are shown. IB_4 stains endothelial cells of capillaries and larger resistance vessels (arrow), though only the former were quantified. Bar = 10 μm. Images were used for stereological assessment in animals exposed to normoxia (Norm) and chronic hypoxia (CH) for 1 −3 weeks. There was no change in LV cardiomyocyte volume (B), total LV capillary length, surface area, or lumen volume (C) after 1 week of normoxia (open bars) or chronic hypoxia (filled bars); 3 week data are not shown. Results obtained from 5 animals/group. *P*-values are for Student's t-test.

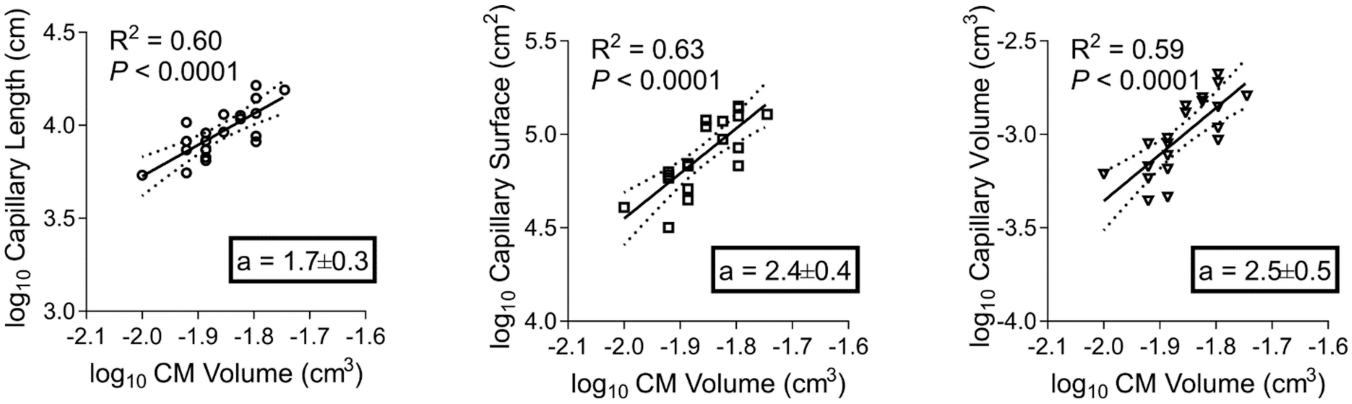

Figure 4. RV microvascular remodeling exceeds RV cardiomyocyte growth

The relationship between RV capillary length (A), surface area (B), or lumen volume (C) and RV cardiac myocyte volume is shown by linear regression; the slope of each line (a = allometry coefficient) represent an estimate of the relative growth, with a slope of 1.0 demonstrating isometry. When compared against one another, the allometry coefficients were not significantly different ($P = 0.34$), suggesting similar rates of relative growth among all microvascular parameters (when compared with CM volume).

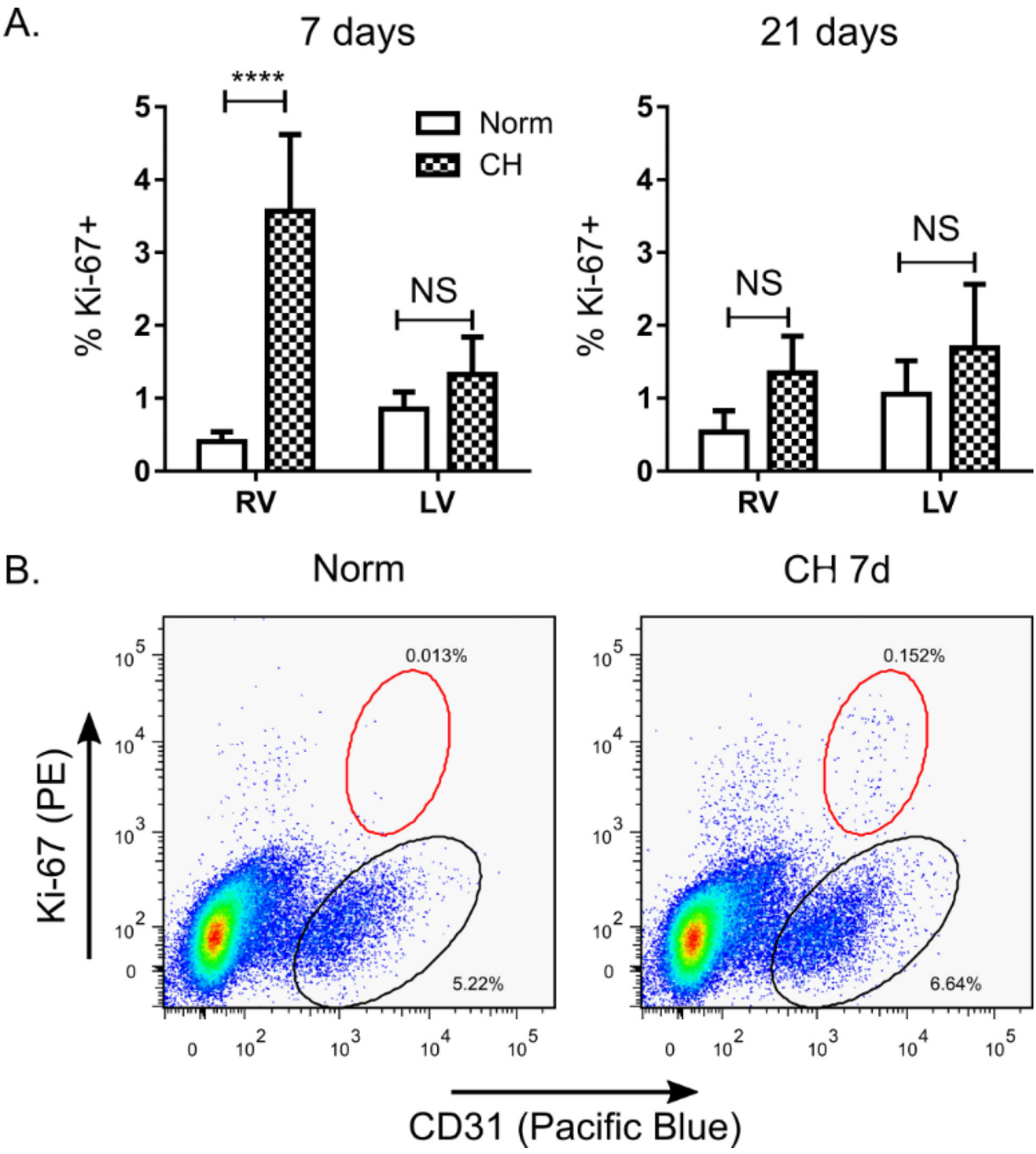

Figure 5. RV angiogenesis is associated with early, RV-specific endothelial cell proliferation

In (A), the percentage $CD31^+$ cells staining positively for Ki-67 in RV and LV/septal preparations are shown after 7 or 21 days of normoxia or CH (n = 6 animals/group). In (B), representative scatter plots from RV samples harvested after 7 days of normoxia (Norm) or hypoxia (CH 7d) are shown. All live cells are shown, with $CD31^+/Ki\text{-}67^-$ cells highlighted by the black circle, and $CD31^+/Ki\text{-}67^+$ cells highlighted in the red circle. **** = $P < 0.0001$; NS = not-significant.

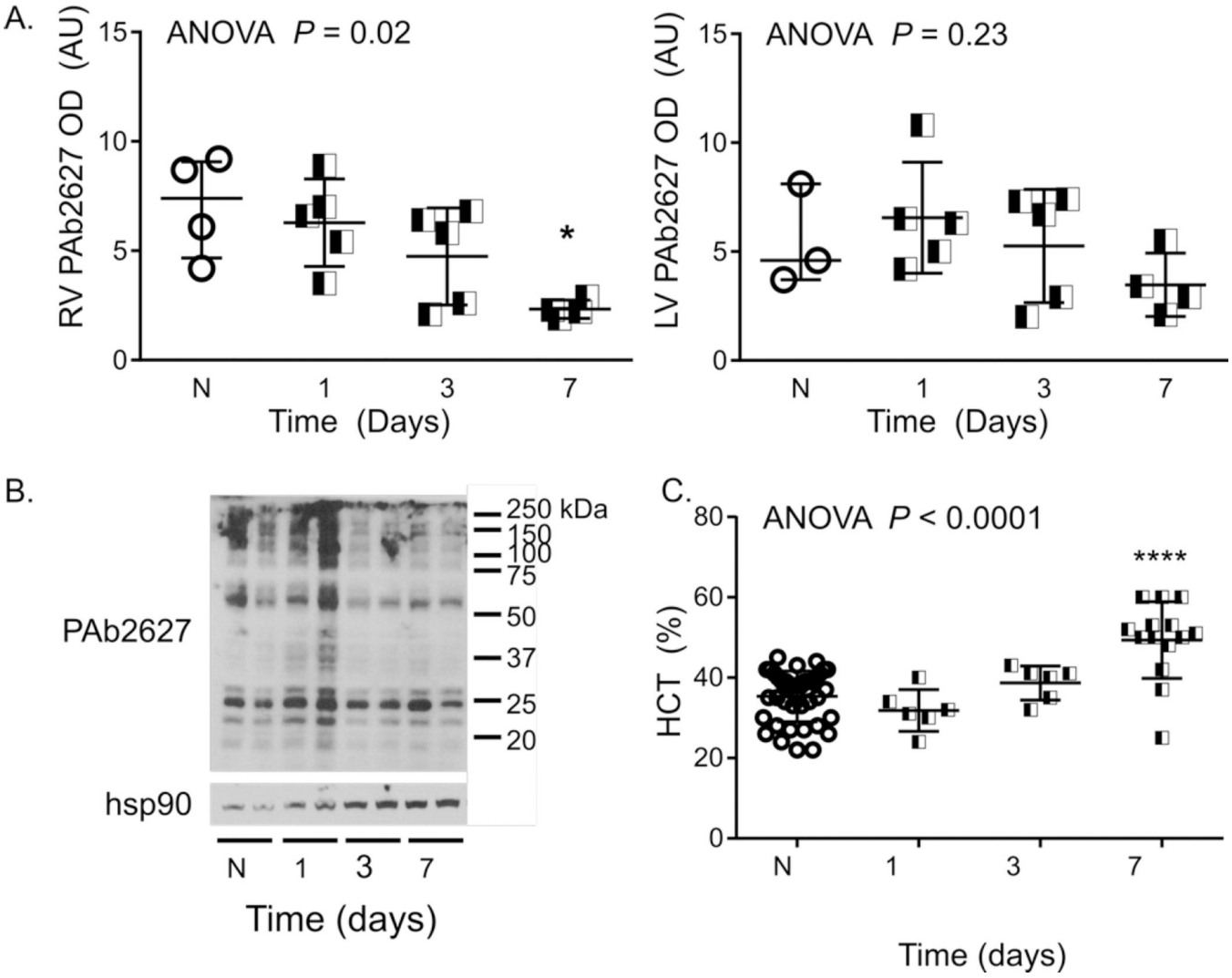

Figure 6. RV tissue hypoxia is a late event in CH-PH induced remodeling

During the first week of CH-PH, semi-quantitative assessment of western blotting showed no evidence of RV or LV tissue hypoxia, as measured by pimonidazole adduct formation (A). In the RV, pimonidazole adduct formation was reduced after 7 days of CH-PH. A representative western blot, showing two animals from each group, is shown in (B). One week was sufficient to generate hypoxia-dependent changes in function of other organs, as evidenced by significant increases in hematocrit (C). *P*-value in (A) is for ANOVA. * = $P < 0.05$; *** = $P < 0.001$; **** = $P < 0.0001$, corrected for multiple comparisons.

A.

VEGFα

CH Time (d)	Δ Exp.	95% CI	*P*
1	1.23	0.89 - 1.78	0.07
3	0.94	0.69 - 1.22	0.47
7	0.94	0.10 - 7.29	0.88
21	0.85	0.02 - 3.42	0.87

VEGFβ

CH Time (d)	Δ Exp.	95% CI	*P*
1	1.13	0.86 - 1.55	0.37
3	0.95	0.76 - 1.22	0.41
7	0.91	0.30 - 3.66	0.70
21	0.64	0.12 - 2.08	0.13

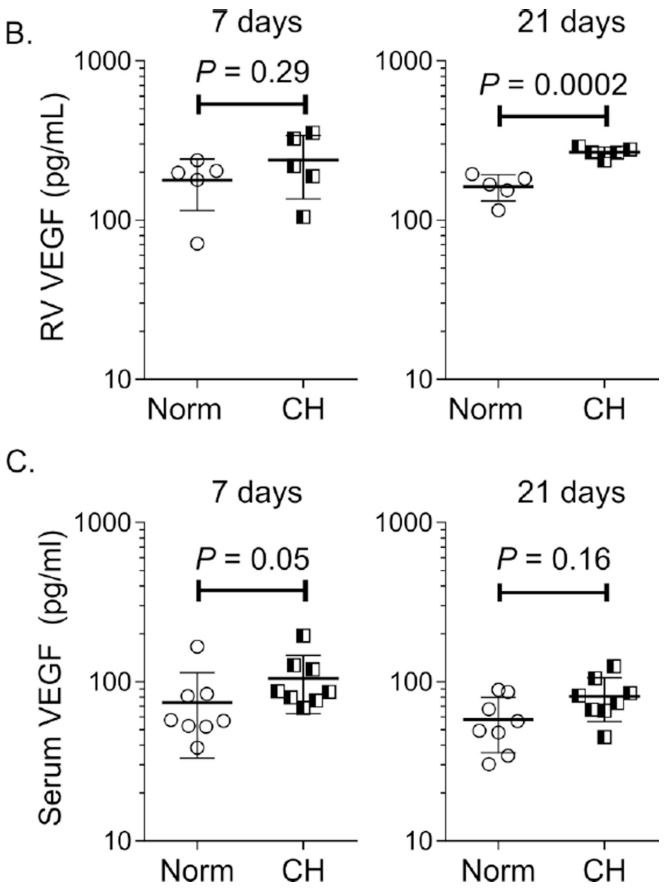

Figure 7. Chronic hypoxia induced RV angiogenesis is not associated with increased VEGF expression

In (A), quantitative PCR demonstrates no change in RV expression of VEGFα or VEGFβ RNA (n=4–6 animals/group). In (B), ELISA demonstrates no change in RV VEGF protein expression after 7 days, but increased RV VEGF after 21 days of CH (n = 5 animals/group). Serum VEGF levels were not significantly increased after 7 or 21 days (n = 8 animals/group).

Microcirculation. Author manuscript; available in PMC 2016 November 01.

Table 1

Chronic hypoxia-induced changes in animal and heart mass.

Time of Exposure													
Variable	**Exp**	**1 day**			**3 days**			**7 days**			**21 days**		
		N	**Mean ± SD**	***P***	**N**	**Mean ± SD**	***P***	**N**	**Mean ± SD**	***P***	**N**	**Mean± SD**	***P***
Mass, t_0 (g)	Norm	6	22.4±1.7	0.40	5	21.3±0.9	0.53	12	24.5±3.3	0.57	6	24.1±1.2	0.09
	CH	6	20.9±3.9		6	21.9±1.9		12	23.7±3.5		6	25.4±1.1	
Mass, t_{sac} (g)	Norm	6	22.7±1.6	0.08	5	22.3±0.9	0.06	23	26.2±3.0	0.04	10	27.8±1.3	0.01
	CH	6	20.8±1.8		6	20.3±1.9		24	24.5±2.6		11	25.8±1.9	
RV/LV+S (mg/mg)	Norm	6	0.227±0.008	0.08	5	0.238±0.013	0.56	23	0.227±0.03	<0.0001	10	0.215±0.03	<0.0001
	CH	6	0.246±0.006		6	0.249±0.012		24	0.285±0.04		11	0.327±0.03	
RV/mass (mg/g)	Norm	6	0.78±0.08	0.14	5	0.78±0.10	0.57	23	0.75±0.12	<0.0001	10	0.74±0.08	<0.0001
	CH	6	0.87±0.10		6	0.82±0.10		24	0.97±0.14		11	1.13±0.14	
LV+S/mass (mg/g)	Norm	6	3.4±0.08	0.53	5	3.3±0.07	1.0	23	3.32±0.23	0.20	10	3.43±0.41	0.97
	CH	6	3.5±0.29		6	3.3±0.14		24	3.40±0.22		11	3.44±0.41	

Mass t_0 = animal mass at start of experiment; Mass t_{sac} = animal mass at time of sacrifice; RV/LV+S = ratio of RV mass to LV/septum mass; RV/mass = ratio of RV mass to body mass; LV+S/mass = ratio of LV+S to body mass.

Table 2

Temporal course for RV angiogenesis and remodeling during CH-PH.

	Exp.	7 days	21 days	ANOVA
L_{cap} (cm)	**Norm**	6822±1379	8289±1513	*P* = 0.75
	CH	10576±2574	12689±3102	
S_{cap} (cm^2)	**Norm**	4.9±1.5	6.5±1.3	*P* = 0.99
	CH	10±3.3	12±1.7	
V_{cap} (cm^3)	**Norm**	0.0006±0.0001	0.0009±0.0002	*P* = 0.86
	CH	0.0013±0.0005	0.0016±0.0003	
V_{myo} (cm^3)	**Norm**	0.012±0.001	0.013±0.002	*P* = 0.88
	CH	0.015±0.001	0.016±0.002	
V_{RV} (cm^3)	**Norm**	0.014±0.002	0.015±0.002	*P* = 0.82
	CH	0.018±0.002	0.019±0.002	

Data are reported as mean ± standard deviation for 5 animals per group. *P*-values are for 2-way ANOVA, comparing effects of hypoxia and time on each parameter. L_{cap} = total capillary length; S_{cap} = total capillary surface area; V_{cap} = total capillary lumen volume; V_{myo} = total myocyte volume; V_{RV} = total RV volume.

Table 3

Correlations between myocardial capillary growth and CM growth.

	L_{cap}	S_{cap}	V_{cap}
RV_{myo} *r*, (*P*)	0.76 (0.00009)	0.79 (0.00008)	0.77 (0.00004)
LV_{myo} *r*, (*P*)	0.23 (0.34)	0.40 (0.08)	0.28 (0.23)

Pearson correlation coefficients (r) and *P*-values are presented for each capillary parameter analyzed and CM volume in the RV (RV_{myo}) and LV (LV_{myo}). L_{cap} = total capillary length; S_{cap} = total capillary surface area; V_{cap} = total capillary lumen volume.

Table 4

Hemodynamics following exposure to normoxia (Norm) or chronic hypoxia (CH) for 7 or 21 days.

	Norm	CH 7 days	CH 21 days	ANOVA	Trend
Parameter					
HR	462.2 ± 58.5	479.6 ± 83.9	477.3 ± 71.4	0.89	0.7
ESP (mm Hg)	19.2 ± 1.6	30.1 ± 5.4	30.6 ± 4.7	<0.0001	<0.0001
EDP (mm Hg)	1.0 ± 0.4	0.7 ± 1.2	2.2 ± 1.1	0.03	0.04
ESV (μL)	31.0 ± 15.4	31.1 ± 14.4	33.6 ± 12.7	0.93	0.73
EDV (μL)	47.2 ± 20.2	45.2 ± 13.4	48.9 ± 19.5	0.93	0.86
SV (μL)	25.5 ± 4.5	23.9 ± 6.2	28.5 ± 6.1	0.33	0.33
CO ($\mu L*min^{-1}$)	11847 ± 2893	11086 ± 2350	13227 ± 1497	0.32	0.28
E_a ($mm\ Hg*\mu L^{-1}$)	0.8 ± 0.2	1.5 ± 0.9	1.2 ± 0.5	0.11	0.22
Systolic Indices					
EF (%)	62.7 ± 22.5	58.4 ± 20.4	65.0 ± 20.3	0.84	0.84
dP/dt_{max} ($mm\ Hg*sec^{-1}$)	1074 ± 291	1909 ± 710	1514 ±331	0.02	0.11
SW (mm Hg*μL)	303.0 ± 45.0	422.8 ± 151.5	430.7 ± 82.3	0.06	0.03
E_{es} ($mm\ Hg*\ \mu L^{-1}$)	2.0 ± 1.3	1.8 ± 1.1	1.6 ± 0.7	0.22	0.52
dP/dt_{max} -EDV ($mm\ Hg*sec^{-1}*\ \mu L^{-1}$)	63.2 ± 49.9	36.5 ± 30.2	22.2 ± 7.4	0.19	0.08
PRSW (mm Hg)	19.9 ± 11.4	24.1 ± 6.6	18.8 ± 5.5	0.54	0.83
Diastolic Indices					
$-dP/dt_{min}$ ($mm\ Hg*sec^{-1}$)	984 ± 204	1907 ± 808	1564 ± 514	0.02	0.07
Tau (ms)	10.7 ± 3.3	7.9 ± 1.9	9.9 ± 2.3	0.13	0.53
RV-PA Coupling					
E_{es}/E_a	2.2 ± 1.3	1.3 ± 0.9	1.5 ± 0.8	0.31	0.27

HR = heart rate; ESP = end-systolic pressure; EDP = end-diastolic pressure; ESV = end-systolic volume; EDV = end-diastolic volume; SV = stroke volume; CO = cardiac output; E_a = arterial elastance; EF = ejection fraction; dP/dt_{max} = maximum rate of pressure change; SW = stroke work; E_{es} = end-systolic elastance; PRSW = preload recruitable stroke work; dP/dt_{min} = minimal rate of pressure change; Tau = isovolumic relaxation constant (Weiss method). Data are from 7 animals/group, except E_{es}, dP/dt_{max}-EDV, PRSW, and E_{es}/E_a which are from 5 animals/group. *P*-values are for one-way ANOVA (ANOVA) with post-hoc testing for linear trend (Trend).

Table 5

RV hypoxia gene expression profile.

CH Time	Gene	Name	Genbank	Fold Δ	*P*
7 days	***Ier3***	**Immediate early response 3**	**NM_133662**	**1.86**	**0.048**
21 days	*Anxa2*	Annexin A2	NM_007585	1.66	0.039
	Bhlhe40	Basic helix-loop-helix family, member e40	NM_011498	2.44	0.013
	Bnip3	BCL2/adenovirus E1B interacting protein 3	NM_009760	2.59	0.021
	Btg1	B-cell translocation gene 1, anti-proliferative	NM_007569	1.79	0.007
	Ccng2	**Cyclin G2**	**NM_007635**	**1.58**	**0.001**
	Egln1	EGL nine homolog 1 (C. elegans)	NM_053207	1.62	0.017
	Ldha	**Lactate dehydrogenase A**	**NM_010699**	**1.59**	**0.007**
	Lgals3	Lectin, galactose binding, soluble 3	NM_010705	2.54	0.041
	Lox	Lysyl oxidase	NM_010728	1.54	0.002
	Map3k1	**Mitogen-activated protein kinase kinase kinase 1**	**NM_011945**	**1.57**	**0.022**
	Ndrg1	N-myc downstream regulated gene 1	NM_008681	1.61	0.027
	P4ha1	Procollagen-proline, 2-oxoglutarate 4-dioxygenase (proline 4-hydroxylase), alpha 1 polypeptide	NM_011030	1.75	0.015
	Per1	Period homolog 1 (Drosophila)	NM_011065	2.02	0.012
	Pfkp	Phosphofructokinase, platelet	NM_019703	2.01	0.003
	Pkm	Pyruvate kinase, muscle	NM_011099	2.05	0.017
	Slc2a1	Solute carrier family 2 (facilitated glucose transporter), member 1	NM_011400	1.60	0.000
	Trp53	Transformation related protein 53	NM_011640	1.64	0.034

Changes in hypoxia- controls is shown after 7 or 21 days. Only genes whose expression was changed >1.5 fold are shown. Only a single hypoxia-dependent gene was upregulated after 7 days of CH-PH (out of 84 possible), while 17 hypoxia-dependent genes were upregulated after 21 days of CH-PH. Genes in bold were upregulated in an RV-specific manner (LV data not shown). N= 3 mice/group.